metals

MDPI

Article

Effect of Mechanical Activation on Spinel Transformation and Chromium Reduction from Ferroalloy Waste Under SHS Conditions

Sanat Tolendiuly *, Nursultan Rakhym, Kaster Kamunur, Sharafkhan Assylkhan, Lyazzat Mussapyrova and Sandugash Tanirbergenova

Institute of Combustion Problems, Bogenbay Batyr St. 172, Almaty 050012, Kazakhstan; rakhymnursultan17@gmail.com (N.R.); kamunur.k@mail.ru (K.K.); sharif29xxxx.10@gmail.com (S.A.); lyazzat.mussapyrova@gmail.com (L.M.); sandu2201@mail.ru (S.T.)

* Correspondence: sanat_tolendiuly@mail.ru

Abstract

Chromium-containing ferroalloy wastes represent an important secondary resource; however, chromium is mainly bound in thermodynamically stable spinel phases, which complicates its reduction. Unlike previous studies focusing on pure oxide systems, this work demonstrates the enhanced destabilization and subsequent reduction of $MgCr_2O_4$ spinel in real ferroalloy wastes under SHS conditions, revealing a non-monotonic relationship between activation time and reduction efficiency. A critical activation threshold (~30 min) was identified, beyond which particle agglomeration suppresses reaction kinetics. Powder mixtures based on HShP and KEK wastes with Al–C–Si reducing agents were mechanically activated for 10–120 min and subsequently subjected to SHS at 950 °C. The combustion parameters, phase composition (XRD), microstructure (SEM), and elemental composition (EDS) were analyzed. The results show a pronounced non-monotonic dependence of combustion temperature and front velocity on activation time, with maximum values at ~30 min (1920 °C and 1.10 mm/s for HShP; 1765 °C and 0.98 mm/s for KEK). XRD analysis indicates that $MgCr_2O_4$ was not detected within the XRD detection limits and that the highest relative amount of metallic chromium phase (~8% for HShP and ~6.8% for KEK) was observed at the same activation time. SEM observations reveal the formation of a more dispersed and porous structure, while EDS indicates an increase in chromium content up to ~15 wt.% in local regions. At longer activation times, overgrinding and agglomeration reduce process efficiency. Mechanical activation enhances chromium reduction through improved mass transfer, with an optimal activation time of ~30 min. The chromium reduction efficiency was evaluated using a semi-quantitative approach based on XRD phase analysis and supported by EDS data, allowing comparative assessment of reduction efficiency rather than absolute extraction values. These results highlight the existence of a critical mechanochemical activation threshold governing the balance between enhanced reactivity and agglomeration effects.

Keywords: mechanical activation; self-propagating high-temperature synthesis; chromium reduction; ferroalloy waste

Check for updates

Academic Editor: Srecko Stopic

Received: 21 April 2026
Revised: 6 May 2026
Accepted: 8 May 2026
Published: 12 May 2026

Copyright: © 2026 by the authors. Licensee MDPI, Basel, Switzerland. This article is an open access article distributed under the terms and conditions of the Creative Commons Attribution (CC BY) license.

1. Introduction

Chromium-containing wastes generated during ferroalloy production represent an important secondary resource due to their significant content of chromium, iron, and

associated elements. In the context of increasingly stringent environmental regulations and the need for sustainable resource utilization, the processing of such technogenic materials has become a critical scientific and technological challenge. Chromium-bearing dusts and slags are now regarded not only as hazardous wastes but also as valuable raw materials for metal recovery. Recent studies have demonstrated that efficient recycling of chromium-containing residues can significantly reduce environmental impact while improving the overall resource efficiency of metallurgical industries [1–3].

In addition, metallurgical wastes have been actively investigated as precursors for functional and refractory materials. It has been shown that waste-derived systems can be effectively transformed into high-temperature-resistant materials with controlled structural and thermal properties, which further expands their technological potential and supports the concept of circular materials processing [4,5].

However, the main difficulty in processing such materials is associated with the presence of chromium in thermodynamically stable spinel phases of the type $(Fe,Mg)(Cr,Al,Fe)_2O_4$, including $MgCr_2O_4$ and $MgAl_2O_4$. These phases exhibit high lattice stability and strong bonding, which significantly hinders chromium reduction, particularly at moderate temperatures. Previous studies on chromium oxide and chromite reduction have shown that these processes are diffusion-controlled and proceed through complex multi-stage mechanisms involving gradual destabilization of the spinel structure and oxygen removal [6–8].

Self-propagating high-temperature synthesis (SHS) represents a promising approach for intensifying reduction processes. In SHS, reactions proceed due to the heat released by exothermic processes and propagate through the material in the form of a combustion wave. This method is characterized by high reaction rates, energy efficiency, and the ability to operate under non-equilibrium conditions, which promote phase transformations and metal recovery [9,10]. In addition to its traditional use in advanced materials synthesis, SHS has also been explored as an environmentally oriented technology for waste processing and resource recovery, highlighting its potential for the treatment of complex technogenic systems [11,12].

The efficiency of SHS strongly depends on the reactivity of the initial charge. Mechanical activation is widely used to enhance powder reactivity through particle refinement and increased specific surface area. Mechanical activation increases powder reactivity by reducing particle size and improving contact between components, which facilitates solid-state reactions [13,14]. Such treatment significantly improves the reactivity of the system and promotes phase transformations. In chromium-bearing systems, such pre-treatment can weaken the spinel structure and facilitate its subsequent reduction. However, excessive activation may lead to particle agglomeration and local sintering, which reduce the effective reactive surface area and hinder mass transfer [15,16].

The balance between structural activation and agglomeration effects plays a decisive role in determining process efficiency. Fundamental aspects of SHS reaction mechanisms and combustion wave propagation have been extensively discussed in the literature [17,18].

Nevertheless, most existing studies are focused on model oxide or chromite systems and do not adequately address real multicomponent ferroalloy wastes, where compositional complexity and phase heterogeneity significantly affect reaction pathways. In particular, the relationship between mechanical activation parameters, spinel phase destruction, and SHS combustion characteristics remains insufficiently understood. The existence of an optimal activation threshold, beyond which further activation leads to a decrease in reduction efficiency due to agglomeration, has not been systematically investigated for real chromium-containing wastes [19,20].

Compared to previous studies focused on model chromium oxide systems, the present work addresses real multicomponent ferroalloy wastes, where phase heterogeneity and

complex composition significantly influence reduction pathways. A key result of this study is the identification of a non-monotonic dependence of chromium reduction on mechanical activation time, with a clearly defined optimal regime (~30 min). This behavior reflects a transition between activation-enhanced reactivity and agglomeration-limited kinetics, which has not been systematically demonstrated for such systems [6,8].

Therefore, the aim of this study is to establish the relationship between mechanical activation time, spinel phase destruction, and chromium reduction efficiency in ferroalloy wastes under SHS conditions, with particular emphasis on identifying the critical activation threshold governing process performance. Preliminary mechanical treatment plays a key role in destabilizing the spinel structure and accelerating subsequent reduction processes.

2. Materials and Methods

The study employed two types of wastes from the Aktobe Ferroalloy Plant (Aktobe, Kazakhstan):

- dry gas-cleaning dust (HShP),
- wet scrubber sludge (KEK).

HShP is characterized by a high content of chromium-containing spinel phases (approximately 60 wt.%), whereas silicate phases dominate in KEK. This fundamental difference significantly affects the efficiency of chromium reduction. The phase compositions of the initial materials are presented in Table 1, which shows that HShP is enriched in chromium-containing spinel phases, while KEK is predominantly composed of silicate phases.

Table 1. Phase composition of chromium-containing wastes.

Type	$MgCr_2O_4$	Mg_2SiO_4	MgO	$CaCO_3$	SiO_2	Fe
HShP	59.5%	30.5%	2.5%	3.5%	2.5%	1.5%
KEK	28.5%	66.2%	–	–	2.3%	3.0%

A base charge composition was selected for the experiments with the following mass fractions: carbon—30 wt.%, aluminum—15 wt.%, silicon—4 wt.%, and the remaining 51 wt.% consisting of chromium-containing waste (HShP or KEK). Aluminum, graphite, and silicon powders were used as reducing agents. To ensure the reliability of the results, each experiment was conducted at least three times. The obtained values were averaged, and the experimental error did not exceed 1–3%.

Mechanical activation was carried out (Figure 1) using a planetary ball mill (PM 100, RETSCH GmbH, Haan, Germany) at a rotation speed of 400 rpm. The powder-to-ball ratio was 1:2. The treatment was performed for 10, 20, 30, 60, 90, and 120 min, ensuring intensive mechanical activation of the powder mixture.

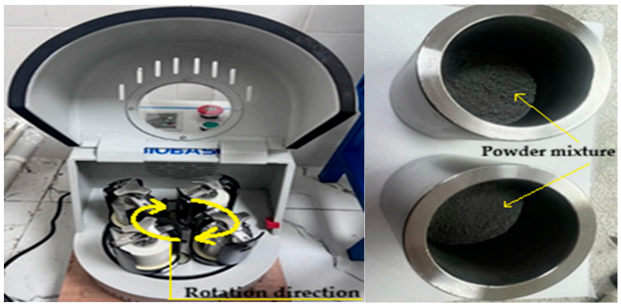

Figure 1. Planetary ball mill (PM 100) used for mechanical activation of powder mixtures prior to SHS processing.

Silica sol was used as a binder to obtain mechanically stable samples. The mixtures were compacted under a pressure of 100 MPa into cylindrical pellets with a diameter of 20 mm using a hydraulic press (PLG-20, LabTools LLC, Saint Petersburg, Russia).

The initiation of SHS occurred upon reaching the ignition temperature, after which the reaction propagated through the sample due to the heat release from exothermic reduction reactions of oxides. The propagation velocity of the combustion front is governed by heat and mass transfer as well as the reactivity of the charge. The synthesis was carried out in a muffle furnace (SNOL 7.2/1100, AB Umega Group, Utena, Lithuania) at 950 °C in air with a holding time of 10–15 min. Under these conditions, the process can be described as thermally assisted SHS, where external heating provides the initiation energy, while subsequent reaction propagation is governed by exothermic processes within the sample. The heating rate prior to ignition corresponds to the standard heating profile of the muffle furnace. Ignition was defined as the moment at which a visible self-propagating combustion front appeared. Combustion temperature values reported in Tables 2 and 3 were obtained experimentally, while combustion front velocity was determined by tracking the propagation of the reaction zone along the sample length. Each experiment was repeated at least three times, and the reported values represent averaged results. Heating led to the initiation of a self-propagating reaction. Figures 2 and 3 illustrate the evolution of the reaction front during the SHS process. As seen from the images, the combustion front propagates uniformly throughout the sample volume, indicating stable SHS behavior and sufficient reactivity of the initial charge. The reaction proceeds in the form of a well-defined combustion zone, confirming that the process occurs in the SHS mode. Arrows indicate the direction of combustion wave propagation during the self-propagating high-temperature synthesis (SHS) process.

Table 2. SHS parameters for HShP.

Mechanical Activation Time, min	Maximum Combustion Temperature, °C	Linear Combustion Velocity, mm/s
10	1780	0.87
20	1815	0.96
30	1920	1.10
60	1790	0.93
90	1775	0.89
120	1730	0.81

Table 3. SHS parameters for KEK.

Mechanical Activation Time, min	Maximum Combustion Temperature, °C	Linear Combustion Velocity, mm/s
10	1640	0.82
20	1665	0.88
30	1765	0.98
60	1710	0.90
90	1680	0.82
120	1650	0.78

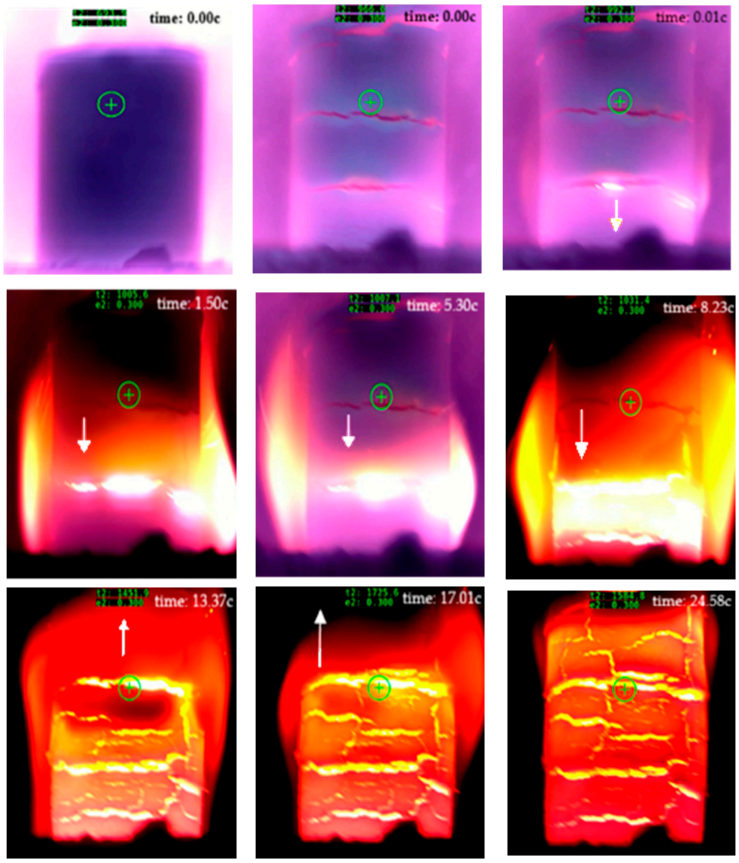

Figure 2. Development of the SHS combustion front in an HShP-based sample.

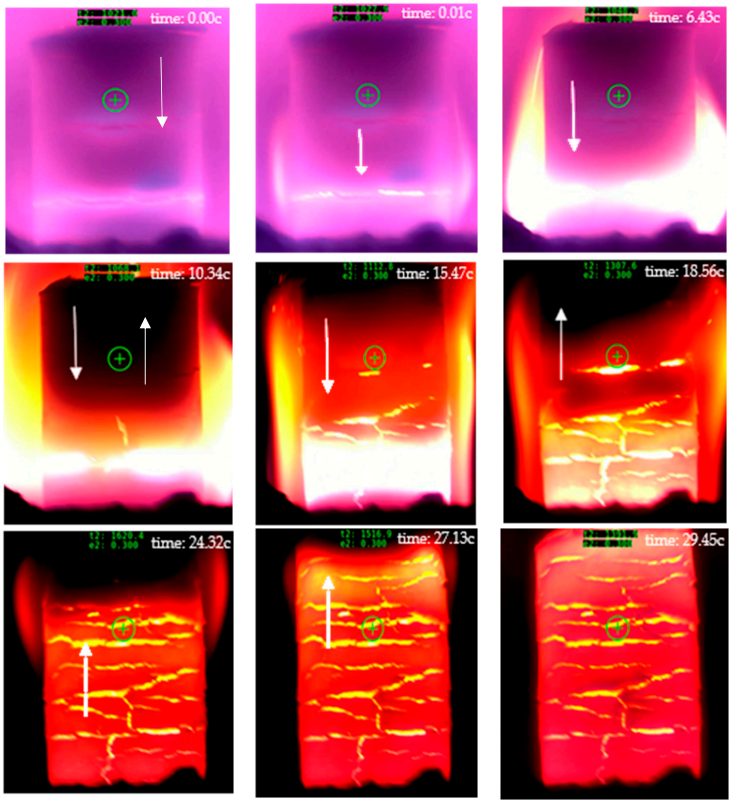

Figure 3. Development of the SHS combustion front in a KEK-based sample.

The observed propagation of a distinct combustion front and the measured velocities (up to ~1.1 mm/s) confirm that the reaction proceeds in a self-propagating mode rather than purely diffusion-controlled furnace reaction.

After synthesis, the samples were characterized using the following techniques:

- X-ray diffraction (XRD),
- scanning electron microscopy (SEM),
- energy-dispersive spectroscopy (EDS).

XRD patterns were obtained using a mini diffractometer (DW-XRD-27, Drawell Scientific Instrument Co., Ltd., Shanghai, China) with Cu Kα radiation. The operating conditions were as follows: tube voltage of 35 kV, tube current of 15 mA, goniometer step size of 0.02° (2θ), and a counting time of 3 s per step.

Morphological features and elemental composition of the samples were analyzed using a desktop scanning electron microscope (Thermo Scientific Phenom XL G2, Thermo Fisher Scientific, Eindhoven, The Netherlands), which enabled high-resolution imaging and local elemental analysis.

Estimation of Chromium Reduction Degree

The relative metallic chromium fraction (R_Crˆmetal) was estimated using a semi-quantitative approach based on the relative content of metallic chromium phases identified by XRD analysis and supported by EDS measurements:

$$R_Cr\hat{}metal = (Cr_metallic/Cr_detected_crystalline_phases) \times 100\%$$

It should be emphasized that this parameter does not represent the absolute chromium recovery yield. Instead, it reflects the relative fraction of chromium present in the metallic state within crystalline phases detectable by XRD. Chromium redistribution into amorphous phases, nanoscale clusters below detection limits, or solid solutions such as $Mg(Al,Cr)_2O_4$ is not captured by this approach. This study should be considered as a semi-quantitative comparative indicator based on XRD phase analysis, rather than an absolute extraction efficiency, due to the absence of a complete material balance.

All experiments were performed under identical conditions to ensure comparability of results. The reported values represent averaged data from at least three independent experiments. The reproducibility of combustion parameters and phase composition was confirmed within experimental uncertainty. In the present study, emphasis is placed on comparative phase analysis under different activation conditions. Therefore, a full material balance or direct chemical quantification of chromium (e.g., ICP-OES or AAS) was not performed.

Such analytical methods are widely used for precise determination of chromium recovery and will be considered in future studies to complement the present results [2].

3. Results

The results of temperature and combustion velocity measurements are presented in Tables 2 and 3.

Analysis of the obtained data (Figures 4 and 5) shows that the dependence of combustion temperature and front propagation velocity on mechanical activation time is non-monotonic. This behavior is consistent with the kinetics of SHS processes, where heat and mass transfer as well as the reactivity of the initial charge play a key role [3,10].

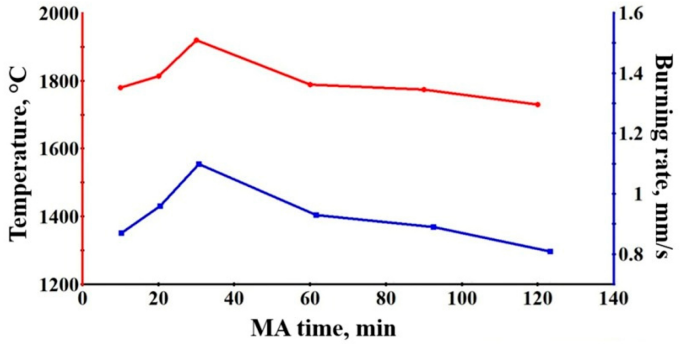

Figure 4. Effect of mechanical activation time on combustion temperature and burning rate (HShP).

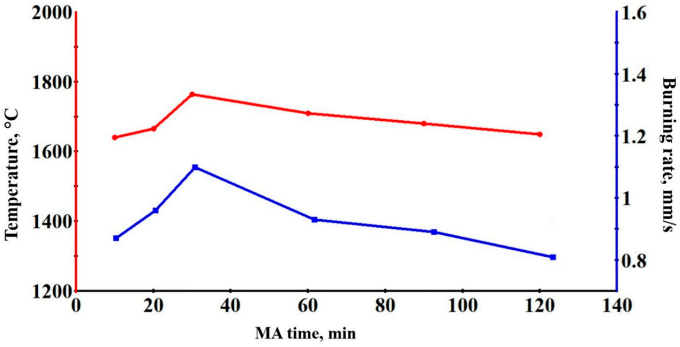

Figure 5. Effect of mechanical activation time on combustion temperature and burning rate (KEK).

The dependence of metallic chromium content on mechanical activation time is presented in Figure 6. It can be seen that both systems exhibit a pronounced maximum at 30 min, corresponding to the highest chromium reduction efficiency. The calculated reduction degree (ηCr) follows the same trend, confirming the optimal activation time of 30 min.

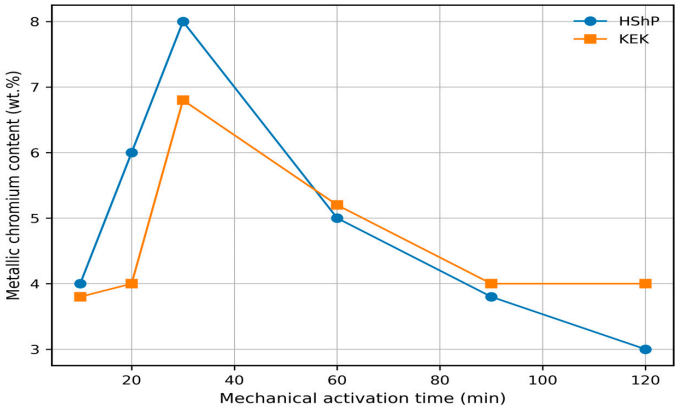

Figure 6. Dependence of relative metallic chromium phase content on mechanical activation time for HShP and KEK-based systems.

The maximum values were observed at a mechanical activation time of 30 min. This behavior is attributed to the fact that, at the initial stages of mechanical activation, destabilization of the spinel structure and an increase in the contact area between reactants occur. At excessive treatment durations (above 30 min), the probability of particle agglomeration increases, which deteriorates diffusion conditions and reduces the reactivity of the system. Thus, the observed optimum mechanical activation time (~30 min) is determined by a balance between surface activation and the onset of agglomeration processes that hinder

reaction kinetics. Similar effects of enhanced reactivity due to mechanical activation have been reported in a number of studies on mechanochemical processes [4–6].

3.1. X-Ray Diffraction

Semi-quantitative phase analysis was performed using the reference intensity ratio (RIR) method. The uncertainty of semi-quantitative phase analysis is estimated to be within ±5%. Although Rietveld refinement can improve the quantitative accuracy of phase analysis, its application in the present study is limited due to the complexity of the multicomponent system and significant peak overlapping. For heterogeneous industrial materials, reliable refinement requires detailed structural modeling and calibration, which is beyond the scope of this work [21].

3.1.1. XRD Analysis Results for HShP-Based Samples

X-ray diffraction (XRD) analysis was performed to evaluate the phase composition of the SHS products and to assess the chromium reduction efficiency as a function of mechanical activation time. Figure 7 shows the effect of mechanical activation time on the phase composition of the SHS products. In this study, the process efficiency was evaluated based on changes in the phase composition of the synthesized products and the content of metallic chromium according to XRD and EDS data. Due to the absence of a complete material balance, it is more appropriate to refer to the chromium reduction efficiency rather than the extraction efficiency in a strict quantitative sense.

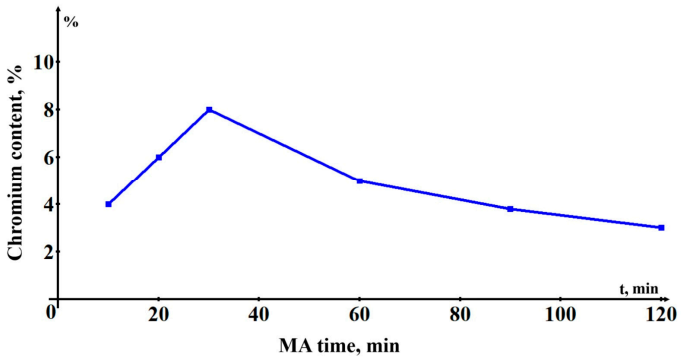

Figure 7. Effect of mechanical activation time on the phase composition of SHS products for HShP-based samples.

According to the XRD data for the series of HShP-based samples, a clear dependence of the phase composition on mechanical activation time is observed. The diffraction patterns reveal the presence of the main phases: $MgAl_2O_4$, Mg_2SiO_4, MgO, SiC, $CaFe_2O_4$, as well as metallic chromium. The quantitative phase composition of the synthesis products is presented in Table 4.

Table 4. Phase composition of SHS products for HShP-based samples.

MA Time, min	$MgAl_2O_4$	Mg_2SiO_4	$MgCr_2O_4$	MgO	SiC	$CaFe_2O_4$	Al	Si	Cr
10	48.0	19.0	8.0	4.0	6.0	5.0	6.0	–	4.0
20	43.0	10.0	15.0	4.0	9.0	5.0	6.0	2.0	6.0
30	53.0	14.0	–	7.0	10.0	8.0	–	–	8.0
60	58.0	13.0	–	7.0	10.0	7.0	–	–	5.0
90	60.0	9.0	–	5.2	11.0	11.0	–	–	3.8
120	68.0	4.0	–	5.0	11.0	9.0	–	–	3.0

Note: deviations from 100% are due to rounding. Estimated uncertainty of phase quantification is ±5%.

The obtained results indicate that mechanical activation promotes the transition of the system from a kinetically limited state to a highly reactive state, leading to the absence of detectable $MgCr_2O_4$ reflections within the XRD detection limits. Such behavior is consistent with systems involving the transformation of spinel structures under mechanical activation followed by reduction [7,8].

At a mechanical activation time of 10–20 min, a noticeable fraction of the initial spinel phase $MgCr_2O_4$ (up to ~15%) remains in the products, indicating incomplete chromium reduction. With an increase in activation time to 30 min, a significant change is observed: the $MgCr_2O_4$ spinel phase is not detected within the detection limits of XRD, while the content of metallic chromium reaches its maximum value (~8%). This suggests the highest relative chromium reduction efficiency under the studied conditions. Considering the increase in metallic chromium content, it can be concluded that the chromium reduction efficiency at 30 min of mechanical activation is substantially higher compared to less activated samples. These results suggest that this activation time corresponds to the most effective transformation of the initial spinel phase and the transition of chromium into the metallic state. This is confirmed by the XRD patterns presented in Figure 8 and is consistent with literature data on the high stability of chromium-containing spinels and the need for additional activation to achieve their reduction [8,9].

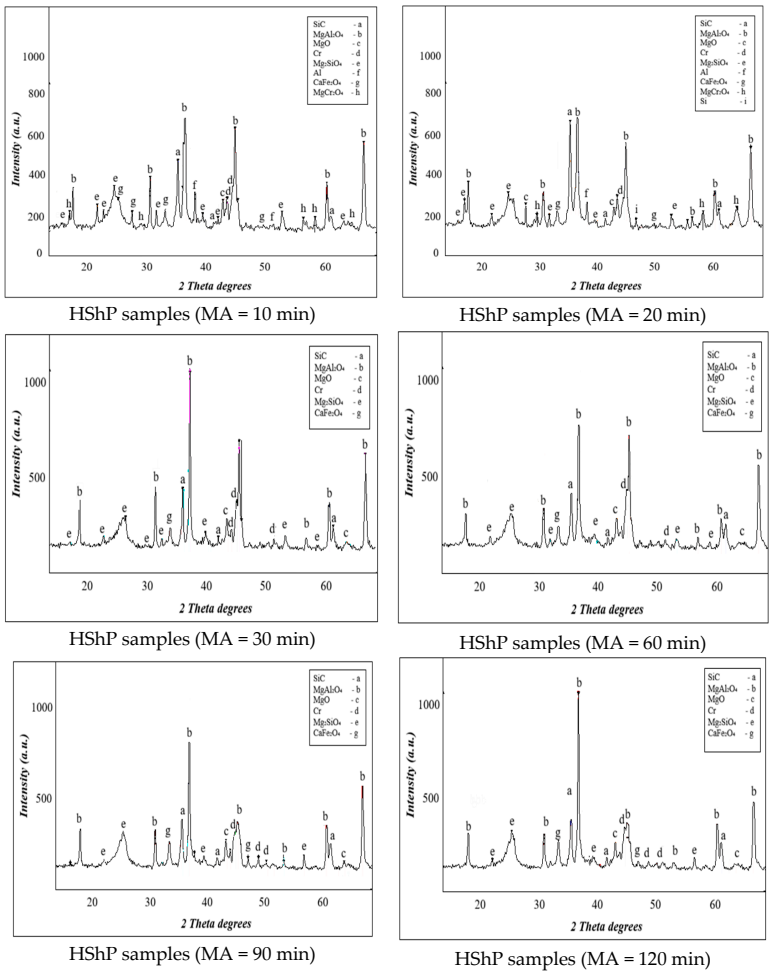

Figure 8. XRD patterns of HShP-based samples at different mechanical activation times.

The apparent disappearance of $MgCr_2O_4$ without proportional formation of metallic chromium suggests redistribution of chromium into multiple sinks: partial reduction to metallic Cr, incorporation into $Mg(Al,Cr)_2O_4$ spinel via Cr^{3+} substitution, retention in

XRD-amorphous or poorly crystalline phases, and formation of nanoscale Cr-containing clusters below XRD detection limits.

With a further increase in mechanical activation time (60–120 min), the content of metallic chromium decreases (down to ~3%), despite the absence of the initial spinel phase. This indicates a redistribution of components among secondary phases. Under these conditions, the formation of oxide and silicate phases ($MgAl_2O_4$, $CaFe_2O_4$), as well as carbides (SiC), is likely enhanced. These phases may partially bind the reduced chromium or limit its segregation in the free metallic form. The formation of $MgAl_2O_4$ is driven by aluminothermic reactions, where aluminum reduces chromium-containing spinel and forms a more stable aluminum-rich spinel phase. $MgAl_2O_4$ is thermodynamically more stable than $MgCr_2O_4$ under reducing conditions due to stronger Al–O bonding, which explains its dominant formation.

3.1.2. XRD Analysis Results for KEK-Based Samples

In contrast to HShP, the KEK-based system is initially characterized by a higher content of silicate phases and a lower fraction of chromium-containing spinel, which is reflected in the reduction results. Figure 9 shows the effect of mechanical activation time on the phase composition of SHS products for KEK. A similar influence of the silicate component on the reduction process has been reported in studies on the processing of chromite materials [7,9].

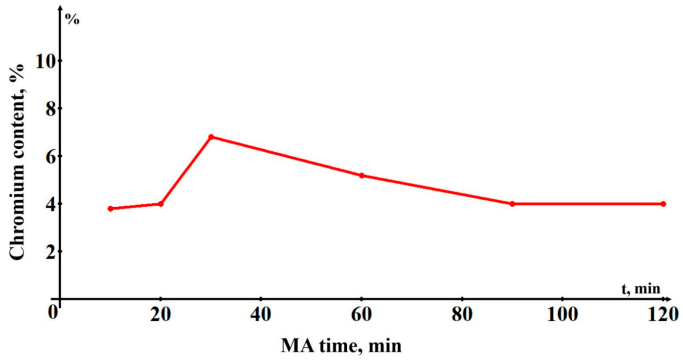

Figure 9. Effect of mechanical activation time on the phase composition of SHS products for KEK-based samples.

The results of the quantitative phase analysis are presented in Table 5.

Table 5. Phase composition of SHS products for KEK-based samples.

MA Time, min	$MgAl_2O_4$	Mg_2SiO_4	$MgCr_2O_4$	MgO	SiC	$CaFe_2O_4$	Al	Si	Fe_3Si	Cr
10	40.0	22.0	14.2	3.0	5.0	3.0	6.0	3.0	–	3.8
20	44.0	17.0	10.0	5.0	8.0	5.0	5.0	2.0	–	4.0
30	68.2	–	–	3.0	10.0	9.0	–	–	3.0	6.8
60	52.8	16.0	3.0	4.0	8.0	4.0	3.0	–	4.0	5.2
90	60.0	10.0	2.0	3.0	8.0	6.0	3.0	–	4.0	4.0
120	64.0	11.0	–	3.0	8.0	5.0	–	–	5.0	4.0

Note: deviations from 100% are due to rounding. Estimated uncertainty of phase quantification is ±5%.

At a mechanical activation time of 30 min, similarly to the HShP system, the maximum content of metallic chromium (~6.8%) is observed. This confirms that the identified trends are of a general nature and are valid for different types of chromium-containing raw materials. This is confirmed by the XRD patterns presented in Figure 10. However, the absolute values are lower, which is attributed to the lower initial chromium content in KEK. In addition, the formation of a silicide phase (Fe_3Si) is detected, which is absent or less

pronounced in the HShP-based system. This indicates a more active involvement of iron and silicon in the reactions during KEK processing.

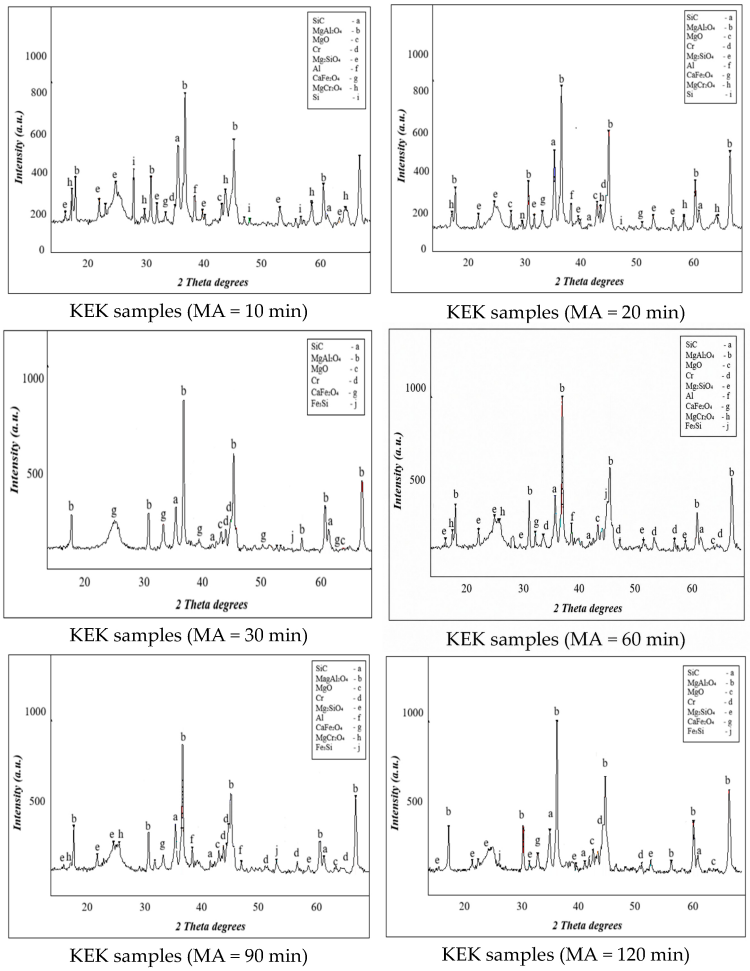

Figure 10. XRD patterns of KEK-based samples at different mechanical activation times.

Thus, the XRD results indicate that for both systems (HShP and KEK), the optimal mechanical activation time is approximately 30 min. Under these conditions, the maximum chromium reduction efficiency is achieved, which is consistent with the temperature and combustion velocity data. The absence of detectable $MgCr_2O_4$ reflections at 30 min suggests substantial transformation of the initial spinel phase within the detection limits of XRD.

3.2. Microstructural Characterization by SEM

To elucidate the reasons for the observed changes in phase composition, a microstructural analysis of the samples was performed. The average particle/agglomerate size after mechanical activation (30 min) was estimated to be significantly smaller compared to non-activated samples, indicating enhanced dispersion and increased reactive surface area. The characteristic particle size decreased significantly after mechanical activation, indicating effective refinement. Figure 11 presents SEM micrographs of the sample surfaces. The images show two types of samples: the initial sample without mechanical activation and the sample subjected to mechanical activation for 30 min. According to the XRD results, the sample mechanically activated for 30 min exhibited the highest formation of the metallic chromium phase.

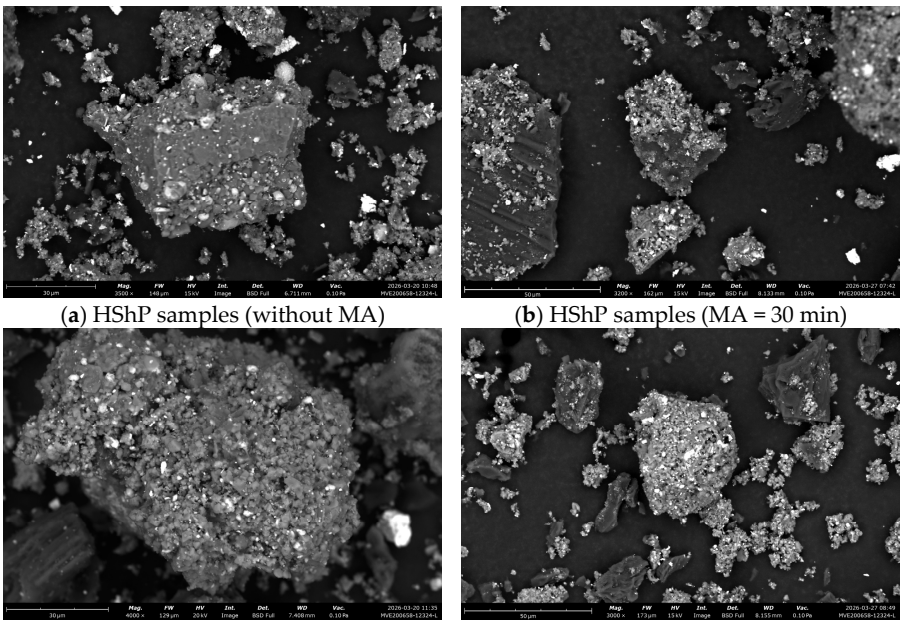

(**a**) HShP samples (without MA) (**b**) HShP samples (MA = 30 min)

(**c**) KEK samples (without MA) (**d**) KEK samples (MA = 30 min)

Figure 11. Microstructure of samples without mechanical activation and after 30 min of treatment.

A comparison of the SEM images (Figure 11) shows that samples without mechanical activation are characterized by a dense and heterogeneous structure with large particle agglomerates. After mechanical activation (30 min), the structure becomes more dispersed, with pronounced porosity and a more uniform phase distribution. At prolonged activation times (>30 min), SEM observations indicate the formation of larger agglomerates and smoother particle surfaces, suggesting cold welding and local densification. Such morphological changes reduce the effective reactive surface area and limit diffusion pathways. Additionally, prolonged mechanical activation may lead to encapsulation of unreacted graphite particles by dense oxide layers, limiting their accessibility for reduction reactions. Although particle size distribution analysis was not performed, SEM observations qualitatively confirm the occurrence of agglomeration at extended activation times. These changes lead to an increase in the contact area between components and facilitate solid-state reactions. They also indicate the development of a reactive surface and the formation of favorable conditions for solid-state processes. These structural modifications explain the increase in combustion temperature and the chromium reduction efficiency at the optimal mechanical activation time. The reduction in particle size and the increase in porosity suggest improved conditions for mass transfer, which is a key factor in accelerating reduction reactions under SHS conditions. It is well known that an increase in dispersion and porosity enhances the reactive surface area and accelerates solid-state processes [4,5].

3.3. Elemental Composition Analysis by EDS

To determine the elemental composition of the synthesis products and to validate the XRD results, energy-dispersive spectroscopy (EDS) was performed on samples without mechanical activation and after 30 min of pre-treatment. The corresponding spectra are presented in Figure 12. EDS results indicate local chromium enrichment rather than uniform bulk reduction, suggesting heterogeneous distribution and possible segregation of metallic chromium. However, EDS does not distinguish between metallic and oxidized chromium states and is therefore used only as a complementary technique to XRD.

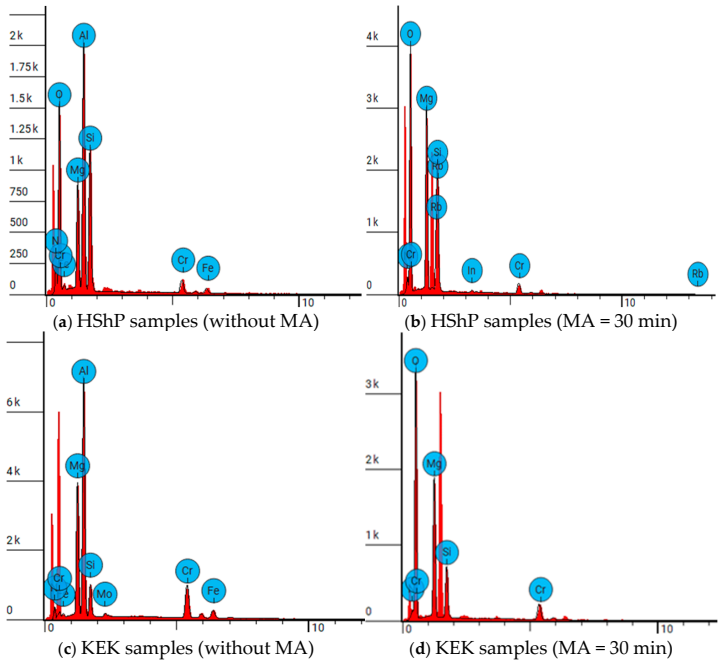

Figure 12. EDS spectra of the SHS synthesis products.

The results of the elemental analysis are presented in Table 6(A)–(D).

The relatively high nitrogen content (Table 6(B)) detected in some EDS measurements is not associated with any nitrogen-containing crystalline phases, as confirmed by XRD analysis. This signal is likely related to surface contamination, adsorbed atmospheric species, or limitations of EDS quantification for light elements.

Table 6. (**A**) Elemental composition of SHS products based on EDS data (HShP samples without mechanical activation). (**B**) Elemental composition of SHS products based on EDS data (HShP samples after 30 min of mechanical activation). (**C**) Elemental composition of SHS products based on EDS data (KEK samples without mechanical activation). (**D**) Elemental composition of SHS products based on EDS data (KEK samples after 30 min of mechanical activation).

(**A**)

Atomic Number	Element Symbol	Element Name	Atomic Concentration, %	Weight Concentration, %
7	N	Nitrogen	10.37	6.60
8	O	Oxygen	43.08	31.30
12	Mg	Magnesium	7.33	8.10
13	Al	Aluminum	20.82	25.50
14	Si	Silicon	14.03	17.90
24	Cr	Chromium	2.67	6.30
26	Fe	Iron	1.70	4.30

(**B**)

Atomic Number	Element Symbol	Element Name	Atomic Concentration, %	Weight Concentration, %
7	N	Nitrogen	14.63	7.31
12	Mg	Magnesium	18.47	16.02
13	Al	Aluminum	46.02	44.24
14	Si	Silicon	9.10	9.11
24	Cr	Chromium	8.15	15.12
26	Fe	Iron	2.92	5.81

Table 6. *Cont.*

(**C**)				
Atomic Number	**Element Symbol**	**Element Name**	**Atomic Concentration, %**	**Weight Concentration, %**
7	N	Nitrogen	4.56	2.80
8	O	Oxygen	62.73	44.00
12	Mg	Magnesium	16.69	17.80
14	Si	Silicon	8.28	10.20
24	Cr	Chromium	2.76	6.30
(**D**)				
Atomic Number	**Element Symbol**	**Element Name**	**Atomic Concentration, %**	**Weight Concentration, %**
7	N	Nitrogen	1.64	1.10
8	O	Oxygen	63.73	48.80
12	Mg	Magnesium	19.85	23.10
14	Si	Silicon	8.55	11.50
24	Cr	Chromium	6.23	15.50

As can be seen from the presented data, the composition of the synthesis products includes the main elements corresponding to the initial charge and reaction products: O, Mg, Al, Si, Cr, and Fe. This is in good agreement with the XRD results. Thus, the EDS data indicate an increase in chromium content in the analyzed regions; however, the metallic state of chromium is confirmed primarily by XRD, consistent with the reduction mechanism established from XRD analysis. These results indicate that mechanical activation affects both phase composition and elemental distribution in the synthesis products. The obtained results are consistent with general concepts of oxide reduction mechanisms under SHS conditions [2,3].

A comparison of the data presented in Figures 4–12 and Tables 2–6 shows good consistency and confirms the identified trends of the process. Overall, the obtained experimental results are in good agreement with current understanding of SHS mechanisms and mechanical activation [1,3,4]. Although elemental mapping was not performed in the present study, the observed compositional heterogeneity suggests that chromium is unevenly distributed within the microstructure. Future work will include elemental mapping to evaluate dispersion and separation feasibility. Thus, EDS results are used exclusively to characterize elemental distribution and should not be interpreted as direct evidence of reduction processes [22].

4. Discussion

The observed non-monotonic behavior results from the competition between two processes: particle refinement, which enhances mass transfer, and agglomeration at prolonged activation times, which reduces the effective reactive surface. Mechanical activation facilitates spinel transformation by improving contact between reactants and enhancing mass transfer. However, excessive activation causes particle welding and agglomeration, reducing reaction efficiency.

Thermodynamically, the transformation can be described by the reaction:

$$MgCr_2O_4 + 2Al \rightarrow MgAl_2O_4 + 2Cr$$

Due to the higher affinity of aluminum for oxygen, this reaction is energetically favorable under SHS conditions. However, not all chromium is reduced to the metallic

state, and part of it remains incorporated into secondary phases. Due to the close ionic radii of Cr^{3+} (0.615 Å) and Al^{3+} (0.535 Å), chromium can partially substitute into the $MgAl_2O_4$ lattice, forming a solid solution Mg $(Al,Cr)_2O_4$. A full quantitative assessment of chromium recovery requires complementary chemical analysis (e.g., ICP-OES), which is beyond the scope of the present study but will be addressed in future work.

From a kinetic perspective, excessive mechanical activation may lead to particle welding and formation of dense agglomerates, which reduce diffusion pathways and limit gas–solid interaction. This results in a decrease in effective reaction surface despite increased initial dispersion [14].

4.1. Analysis of Results for the Series of HShP-Based Samples

For the sample without mechanical activation (Figure 11a, Table 6(A)), a relatively low chromium content is observed: Cr ~6.3 wt.%. At the same time, a significant fraction corresponds to oxygen (~31.3 wt.%) and aluminum (~25.5 wt.%), indicating the predominance of oxide phases. After mechanical activation for 30 min (Figure 11b, Table 6(B)), noticeable changes in composition are observed: the Cr content increases to ~15.1 wt.%, the fractions of Mg and Al increase, while the relative oxygen content decreases. Such redistribution indicates a deeper reduction of chromium and a shift in the phase composition toward a higher fraction of metallic or weakly oxidized phases.

4.2. Analysis of Results for the Series of KEK-Based Samples

A similar trend is observed for the KEK-based samples. For the sample without mechanical activation (Figure 11c, Table 6(C)), the Cr content is ~6.3 wt.%, while a high oxygen fraction (~44 wt.%) indicates the predominance of oxide and silicate phases. After mechanical activation for 30 min (Figure 11d, Table 6(D)), the Cr content increases to ~15.5 wt.%. The high oxygen content (~48.8 wt.%) is retained, which is associated with the presence of silicate and oxide phases characteristic of KEK. Thus, despite the more "inert" initial composition, mechanical activation also leads to a significant increase in the fraction of reduced chromium.

The obtained results are in good agreement with the XRD data, where the maximum content of metallic chromium is also observed at a mechanical activation time of approximately 30 min. The increase in Cr content according to EDS confirms that this regime provides the most favorable conditions for reduction reactions in the system. Detected minor elements such as Mo, Rb, and in are attributed to instrumental or sample-holder-related artifacts and were excluded from further quantitative interpretation.

The most pronounced effect is observed at a mechanical activation time of 30 min, which is consistent with the XRD results and SHS parameters. A comparison of XRD, SEM, and EDS results shows good agreement between the methods. The increase in SHS temperature and combustion velocity is accompanied by changes in microstructure and an increase in the content of metallic chromium, indicating a combined effect of mechanical activation on the reduction process. The higher reduction efficiency observed in HShP compared to KEK is attributed to the higher initial content of chromium-bearing spinel phases, which provide a more favorable thermodynamic driving force for reduction. In contrast, the silicate-rich composition of KEK leads to dilution of reactive components and formation of stable secondary phases.

5. Conclusions

This study demonstrates the influence of mechanical activation on the reduction of chromium from complex ferroalloy wastes under SHS conditions, particularly highlighting the critical role of activation-induced changes in phase composition. First, the conducted

experiments demonstrated that preliminary mechanical activation has a decisive influence on the solid-state reduction of chromium under SHS conditions.

It was established that the dependence of combustion temperature and reaction front propagation velocity on mechanical activation time exhibits a pronounced non-monotonic behavior. For both systems—HShP- and KEK-based—the maximum values are achieved at a mechanical activation time of approximately 30 min. Under these conditions, the combustion temperature reaches ~1920 °C for HShP and ~1765 °C for KEK, while the front propagation velocity is 1.10 and 0.98 mm/s, respectively.

XRD results showed that the highest chromium reduction efficiency is achieved at this activation time. For HShP-based samples, this is evidenced by the absence of detectable $MgCr_2O_4$ reflections within the XRD detection limits and the maximum content of metallic chromium (~8%). For KEK, the maximum Cr content (~6.8%) is also observed; however, the values are lower due to the lower initial chromium content and the predominance of silicate phases.

At the optimal activation time, a more dispersed and porous structure is formed, with an increased interfacial contact area, which promotes enhanced reactivity of the system.

EDS analysis revealed an increase in chromium content in the analyzed regions after mechanical activation. For HShP-based samples, the Cr content increases from ~6.3 to ~15.1 wt.%, while for KEK-based samples it reaches ~15.5 wt.% at an activation time of 30 min. This supports the enhanced chromium reduction behavior observed after mechanical activation.

It is shown that with an increase in mechanical activation time beyond 30 min, the process efficiency decreases. This is associated with overgrinding and particle agglomeration, which deteriorate heat and mass transfer conditions and lead to a decrease in the chromium reduction efficiency.

A comparative analysis of the two types of raw materials showed that HShP is a more promising material for chromium extraction under SHS conditions, as it is characterized by a higher initial content of spinel phases and, consequently, provides a higher yield of metallic chromium.

The results indicate that the optimal mechanical activation time for the studied system is approximately 30 min, at which the best combination of combustion parameters, phase composition, and microstructure of the synthesis products is achieved.

Mechanical activation was shown to significantly influence SHS combustion behavior and the relative chromium reduction efficiency.

Author Contributions: Conceptualization, S.T. (Sanat Tolendiuly); methodology, S.T. (Sanat Tolendiuly), S.T. (Sandugash Tanirbergenova) and L.M.; validation, L.M. and S.A.; formal analysis, S.T. (Sanat Tolendiuly), L.M. and S.A.; investigation, S.A. and N.R.; resources, K.K.; data curation, S.A.; writing—original draft preparation, S.T. (Sanat Tolendiuly) and N.R.; writing—review and editing, S.T. (Sanat Tolendiuly), N.R., S.T. (Sandugash Tanirbergenova), L.M. and K.K.; visualization, S.T. (Sanat Tolendiuly), S.T. (Sandugash Tanirbergenova) and L.M.; supervision, K.K.; project administration, S.T. (Sandugash Tanirbergenova); funding acquisition, S.T. (Sandugash Tanirbergenova). All authors have read and agreed to the published version of the manuscript.

Funding: This research was funded by the Science Committee of The Ministry of Science and Higher Education of the Republic of Kazakhstan (Grant No. BR28713557).

Data Availability Statement: The original contributions presented in this study are included in the article. Further inquiries can be directed to the corresponding author.

Conflicts of Interest: The authors declare no conflicts of interest.

Abbreviations

The following abbreviations are used in this manuscript:

SHS	Self-propagating high-temperature synthesis
MA	Mechanical activation
XRD	X-ray diffraction
SEM	Scanning electron microscopy
EDS	Energy-dispersive spectroscopy
HShP	Dry gas-cleaning dust
KEK	Wet scrubber sludge

References

1. Xu, J.; Liu, M.; Ma, G.; Zheng, D.; Zhang, X.; Hou, Y. Valuable Recovery Technology and Resource Utilization of Chromium-Containing Metallurgical Dust and Slag: A Review. *Metals* **2023**, *13*, 1768. [CrossRef]
2. Gu, F.; Zhang, Y.; Su, Z.; Tu, Y.; Liu, S.; Jiang, T. Recovery of Chromium from Chromium-Bearing Slags Produced in the Stainless-Steel Smelting: A Review. *J. Clean. Prod.* **2021**, *296*, 126467. [CrossRef]
3. Sariyev, O.; Tolymbekova, L.; Dossekenov, M.; Kelamanov, B.; Yessengaliyev, D.; Davletova, A.; Abdirashit, A. Analysis and Chromium Recovery from Ferrochrome Waste (Stockpiled Refined Ferrochrome Slags). *Metals* **2025**, *15*, 740. [CrossRef]
4. Fomenko, S.M.; Akishev, A.; Tolendiuly, S. Thermal Flows Influence on the Change of Temperature Stresses in Surface and Inner Layers of Refractories. *Mater. Today Proc.* **2020**, *33*, 1853–1858. [CrossRef]
5. Fomenko, S.M.; Tolendiuly, S.; Akishev, A.K.; Almagambetov, M.; Yeskendirov, R. The Technology for Producing Refractory Products Based on Metallurgical Production Waste. *AIP Conf. Proc.* **2021**, *2380*, 040003. [CrossRef]
6. Mori, T.; Yang, J.; Kuwabara, M. Mechanism of Carbothermic Reduction of Chromium Oxide. *ISIJ Int.* **2007**, *47*, 1387–1393. [CrossRef]
7. Chakraborty, D.; Ranganathan, S.; Sinha, S.N. Carbothermic Reduction of Chromite Ore under Different Flow Rates of Inert Gas. *Metall. Mater. Trans. B* **2010**, *41*, 10–18. [CrossRef]
8. Hu, X.; Teng, L.; Wang, H.; Ökvist, L.S.; Yang, Q.; Björkman, B.; Seetharaman, S. Carbothermic Reduction of Synthetic Chromite with/without the Addition of Iron Powder. *ISIJ Int.* **2016**, *56*, 2147–2155. [CrossRef]
9. Varma, A.; Lebrat, J.-P. Combustion Synthesis of Advanced Materials. *Chem. Eng. Sci.* **1992**, *47*, 2179–2194. [CrossRef]
10. Munir, Z.A.; Anselmi-Tamburini, U. Self-Propagating Exothermic Reactions: The Synthesis of High-Temperature Materials by Combustion. *Mater. Sci. Rep.* **1989**, *3*, 277–365. [CrossRef]
11. Cao, G.; Orrù, R. Self-Propagating Reactions for Environmental Protection: State of the Art and Future Directions. *Chem. Eng. J.* **2002**, *87*, 239–249. [CrossRef]
12. Xanthopoulou, G.; Vekinis, G. An Overview of Some Environmental Applications of Self-Propagating High-Temperature Synthesis. *Adv. Environ. Res.* **2001**, *5*, 117–128. [CrossRef]
13. Suryanarayana, C. Mechanical Alloying and Milling. *Prog. Mater. Sci.* **2001**, *46*, 1–184. [CrossRef]
14. Baláž, P. *Mechanochemistry in Nanoscience and Minerals Engineering*; Springer: Berlin/Heidelberg, Germany, 2008. [CrossRef]
15. Apaydin, F.; Atasoy, A.; Yildiz, K. Effect of Mechanical Activation on Carbothermal Reduction of Chromite with Graphite. *Can. Metall. Q.* **2011**, *50*, 113–118. [CrossRef]
16. Davies, J.; Tangstad, M.; Ringdalen, E.; Beukes, J.P.; Bessarabov, D.; du Preez, S.P. The Effect of Pre-Oxidation on the Reducibility of Chromite Using Hydrogen: A Preliminary Study. *Minerals* **2022**, *12*, 911. [CrossRef]
17. Varma, A.; Rogachev, A.S.; Mukasyan, A.S.; Hwang, S. Combustion Synthesis of Advanced Materials: Principles and Applications. *Adv. Chem. Eng.* **1998**, *24*, 79–226. [CrossRef]
18. Mukasyan, A.S.; Rogachev, A.S. Discrete reaction waves: Gasless combustion of solid powder mixtures. *Prog. Energy Combust. Sci.* **2008**, *34*, 377–416. [CrossRef]
19. Boldyrev, V.V. Mechanochemistry and mechanical activation of solids. *Russ. Chem. Rev.* **2006**, *75*, 177–189. [CrossRef]
20. Merzhanov, A.G. Self-Propagating High-Temperature Synthesis: Twenty Years of Search and Findings. In *Combustion Science and Technology*; ISMAN: Chernogolovka, Russia, 1989; 91p.
21. Young, R.A. (Ed.) *The Rietveld Method*; Oxford University Press: Oxford, UK, 1993; 298p.
22. Goldstein, J.I.; Newbury, D.E.; Joy, D.C.; Lyman, C.E.; Echlin, P.; Lifshin, E.; Sawyer, L.; Michael, J.R. *Scanning Electron Microscopy and X-Ray Microanalysis*, 3rd ed.; Springer: New York, NY, USA, 2003. [CrossRef]

Disclaimer/Publisher's Note: The statements, opinions and data contained in all publications are solely those of the individual author(s) and contributor(s) and not of MDPI and/or the editor(s). MDPI and/or the editor(s) disclaim responsibility for any injury to people or property resulting from any ideas, methods, instructions or products referred to in the content.